Nuclear Materials and Energy 30 (2022) 101093

Contents lists available at ScienceDirect

Nuclear Materials and Energy

journal homepage: www.elsevier.com/locate/nme

Irradiation effects in tungsten—From surface effects to bulk mechanical properties

J. Riesch [a,*], A. Feichtmayer [a,b], J.W. Coenen [c,d], B. Curzadd [a], H. Gietl [e], T. Höschen [a], A. Manhard [a], T. Schwarz-Selinger [a], R. Neu [a,b]

[a] Max-Planck-Institut für Plasmaphysik, 85748 Garching, Germany
[b] Technische Universität München, 85748 Garching, Germany
[c] Forschungszentrum Jülich GmbH, Institut für Energie- und Klimaforschung – Plasmaphysik, 52425 Jülich, Germany
[d] Department of Engineering Physics, University of Wisconsin - Madison, Madison, WI 53706, USA
[e] Materials Science and Technology Division, Oak Ridge National Laboratory, Oak Ridge, TN 37831, USA

ARTICLE INFO

Keywords:
Tungsten
Wire
Ion irradiation
Tensile test
Embrittlement
Ductility

ABSTRACT

Advanced materials such as tungsten fibre-reinforced composites allow to overcome severe weaknesses of the baseline materials for plasma-facing components — copper and tungsten. The effect of the fusion environment on the mechanical properties of these materials, e.g. the embrittlement by neutron irradiation, plays a key role for the development of future fusion reactors. To simulate this effect, high-energy ions are used as a substitute for the displacement damage by neutrons. We propose the use of very fine tungsten wire as a possibility of studying the influence of irradiation damage on the mechanical properties. This is possible as they allow full-depth irradiation of almost the entire volume despite the limited penetration depth of ions. Geometrical size effects are mitigated due to the nanoscale microstructure of the wire. In addition, similar wire is used in tungsten fibre-reinforced composites. Thus, the investigation of irradiated wire can directly be used for the prediction of the bulk composite properties. For the proof of this concept tungsten wire with a diameter of 16 μm was electrochemically thinned to 5 μm and irradiated with 20.5 MeV W^{6+} ions. The mechanical properties were subsequently determined by macroscopic tensile testing. Irradiation to 0.3, 1 and 9 dpa did not lead to a change of the mechanical behaviour. Both strength and ductility, the latter indicated by the reduction of area, were similar to the as-fabricated state.

1. Introduction

For next step fusion reactors such as DEMO [1] or a fusion power plant, the requirements for first wall materials will be more stringent than for current devices and will require for advanced materials [2,3]. Currently favoured candidate materials such as tungsten (W) for the plasma-facing parts and copper (Cu) for cooling structures have severe weaknesses. Tungsten is brittle at low temperature and susceptible to embrittlement by thermal overload [4] and/or irradiation [5,6]. In the case of copper, the strength is strongly reduced above 300 °C [7]. A promising way to improve upon the properties of conventional materials is reinforcement with high-strength, ductile drawn W wire [8]. By using potassium doped tungsten wire these favourable properties are preserved up to very high temperatures [9]. In tungsten fibre-reinforced tungsten composites (W_f/W), the W wire is embedded in a W matrix produced by powder metallurgy or a chemical vapour deposition process. An engineered interface between wire and matrix, e.g. a thin oxide layer, enables controlled deflection of growing cracks. This activates energy dissipating mechanisms which allow the relaxation of stress peaks, increasing the resistance to fracture [10,11], as in ceramic fibre-reinforced ceramics (see e.g. [12]). Tungsten wire is also used to reinforce copper materials in order to improve their strength at elevated temperature [13]. W and Cu combine very well as they form a strong bond without forming a solid solution or intermetallic phases [14].

In a future fusion reactor, high neutron fluxes originating from the D-T nuclear reaction will occur [15]. The impinging neutrons will cause displacement damage and transmutation, possibly leading to a significant change in the material properties. Exposure of metals to irradiation in general leads to an increase in strength accompanied by a decrease of ductility [16]. This behaviour is known as irradiation hardening and can lead to a complete loss of ductility in bcc metals. The reason for this hardening is the production of various defects in the lattice. Beside the change in mechanical properties, an increase in

* Corresponding author.
E-mail address: johann.riesch@ipp.mpg.de (J. Riesch).

https://doi.org/10.1016/j.nme.2021.101093
Received 19 August 2021; Received in revised form 4 November 2021; Accepted 17 November 2021
Available online 30 December 2021

the hydrogen isotope retention is of concern [17]. In a fusion reactor, the materials are subjected to an energy spectrum of neutrons reaching up to an energy of 14 MeV (see e.g. [18]). Currently, there is no facility available to test under these conditions. Alternatively, two methods are used to simulate the expected effects: neutron irradiation in a fission reactor and irradiation by high-energy ions. Although fission can be readily used [19] there are concerns about the differences in the energy spectrum [20]. Further, due to the need of long irradiation times and the activation of samples, the costs and cycle times (from outlining experiments until receiving results) are high [16]. On the other hand, the use of ion beams allows fast iterations which are helpful in material development programmes. Here, the damage created by heavy ions is expected to produce dense cascades similar to neutron induced damage [16,21]. The conditions during ion irradiation are easily controlled, allowing defined energies, dose rates and sample temperatures [22]. Furthermore, it allows high dose rates up to 10 dpa h^{-1} if using heavy ions (for comparison, dose rates in fission reactors are in the range of 1 dpa $year^{-1}$ [23]). Compared to neutron irradiation, activation of the samples is absent for heavy ions which makes subsequent testing and characterisation easier (no hot cells required). In contrast to neutron irradiation no transmutation occurs for heavy ions. A large drawback for the study of structural material is the shallow penetration depth of a few nm to approximately 100 μm (for light ions). The implantation of impurities is avoided by damaging the material with the same element (i.e. self-ion implantation). For 20.5 MeV W^{6+} ions the damaging zone reaches the peak damage at around 1.3 μm in W as calculated by SRIM [24] (profile shown in Fig. 3(a), details in [25]). A comprehensive overview about the use of ion irradiation as a substitute for neutron irradiation is given by Was et al. [16,22] and in the ASTM Standard E521-16 [26].

As a consequence of the shallow penetration depth, the mechanical properties are frequently investigated by nano-indentation or micro-mechanical testing [27]. During nanoindentation the affected volume is typically larger than the irradiation depth, which complicates the determination of the irradiation effect on the mechanical properties [28]. In micro-mechanical testing, the actual sample size is often on the same length scale as that of the microstructural features. As a consequence, the results of those tests represent the properties of these features . Using them for the prediction of general material properties is challenging [29].

In this contribution, fine-grained tungsten wire is proposed as a polycrystalline model system to avoid this problem. We assess the mechanical properties after ion irradiation by tensile testing to investigate ductility and strength directly. The first results of irradiation by W^{6+} up to 9 dpa are presented.

2. Tungsten wire — a polycrystalline model system

Tungsten wire is produced by multi step drawing and available down to a diameter of 16 μm (as produced by drawing). The large deformation leads to a very fine microstructure. In Fig. 1, the longitudinal sections of a tungsten wire with a diameter of 150 μm (left), as frequently used in W_f/W composites, and of a wire with a diameter of 16 μm (right) are shown. Especially the grain size of the 16 μm wire is so small that even within the damage range of heavy ions many grains are in the affected volume. In [30], it was shown that wires with diameters of 150 μm and 16 μm, which was electrochemically thinned to 5 μm, show very similar tensile behaviour and ductility (considering the reduction in area as the characteristic property). Assuming a penetration depth of 2.3 μm (compare Fig. 3) for 20.5 MeV W^{6+} ions and irradiation from two opposing directions it is possible to irradiate almost the entire volume of 5 μm thick wire (see Table B.3 for concrete values).

Tungsten wire has a high strength and is ductile at room temperature (RT). The 150 μm wire has a strength around 3000 MPa, which increases to 4500 MPa for 16 μm wire [30]. During a tensile test, W wire

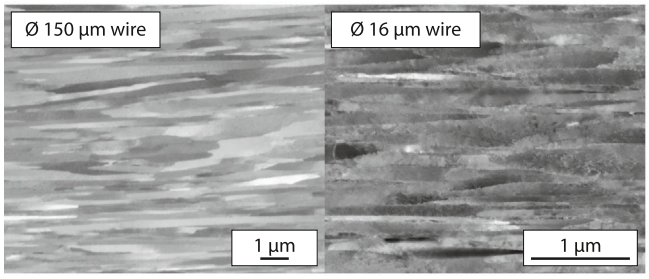

Fig. 1. Scanning electron microscopy (SEM) pictures of the longitudinal section of tungsten wire with a diameter of 150 μm (left) and 16 μm (right) (Z contrast using the circular backscatter detector (CBS)). Both sections were prepared by a focussed ion beam polishing within the SEM. The magnifications are chosen to show similar sizes for the grains but note the differences in the scale bars (ratio 1:3.5).

shows a pronounced ductile behaviour expressed in strong necking. The reduction in area is a good measure for the ductility [31]. Tensile tests can therefore be used to determine the strength and ductility and their possible reduction by irradiation effects.

Tungsten wire is a standardized industrial product originally developed for illumination applications [32]. This ensures the availability of well-defined samples with a well-controlled quality. Variability in sample quality is thus reduced and a correlation between individual tests is possible.

The as-fabricated fine-grained microstructure of a tungsten wire is highly distorted [33,34]. Due to the drawing process the grains are curled forming the so called van Gogh structure [35]. By annealing, the microstructure can be modified in a very controlled way [33,34]. At moderate temperatures (1000 °C for pure W wire and 1600 °C for K-doped W wire) the curling as well as most of the dislocations are removed. Although the grain size increases slightly, the elongated fine grain structure is maintained. Annealing at high temperature leads to massive grain growth producing a few large grains (1600 °C for pure W wire and 2300 °C for K doped W wire [9]). It can even yield a single grain across the whole diameter.

3. Experimental

In this section we describe the experimental procedure. Detailed values and results for the individual samples are given in section 4 and Table 1. Samples were made from potassium doped (60–75 ppm) drawn tungsten wire produced by OSRAM GmbH, Schwabmünchen Germany. The wire had a nominal diameter of 16 μm and was cut to pieces with a length of 80–90 mm, referred to in the following as fibres. For handling, the fibres were attached to a paper frame by a two component epoxy (UHU Plus endfest 300). A mounting jig was used to held the fibres straight and in position during gluing. In Fig. 2, a picture of such a frame is shown together with the corresponding dimensions.

Electrochemical thinning was used to reduce the diameter to approximately 5 μm in the centre of the fibre (see Fig. 2, right). For that, the fibre was coated by an insulating protective lacquer (Plastik70 by Kontakt Chemie) except for a 2 mm long region in the centre. It was then clamped on one end of the frame by a crocodile clamp and inserted into an electrolyte (mixture of NaOH (9 g), H_2O (300 g) and glycerine (450 g); details in [36]) for electrochemical thinning. The electrical contact was ensured by a left over wire piece at the top end of the frame. Applying a DC voltage of 7 V while constantly rotating the sample inside a cylindrical cathode leads to a uniform removal of material in the uncoated area until the target diameter is reached. Due to the ratio of 10 between the cross-sectional area in the thinned and unthinned region the fracture will occur in this zone. This will even be the case if a significant increase in strength caused by irradiation hardening would occur. The length of the thinned area defines the gauge length. Contaminations

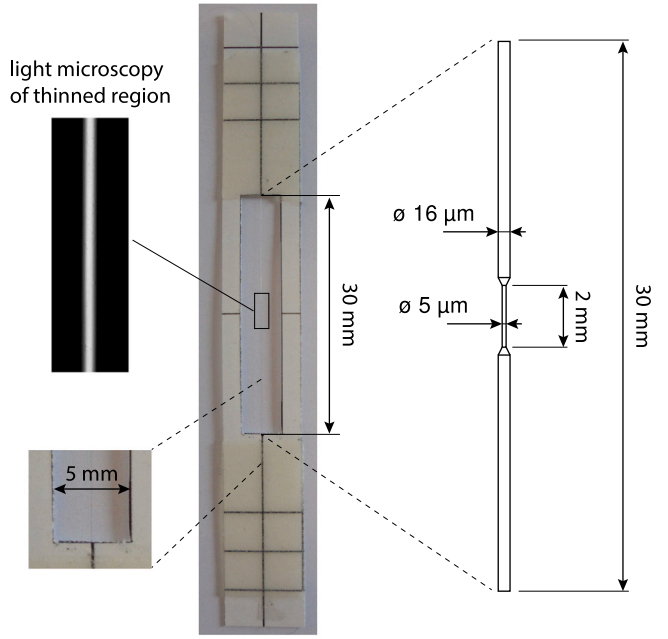

Fig. 2. Photo of a paper frame containing a 16 µm W wire attached by a two component epoxy (UHU Plus endfest 300). Extract shows schematically the geometry of the testing area where the centre part is thinned to a diameter of 5 µm over a length of 2 mm. On the left side an optical microscopy image of the thinned region is shown.

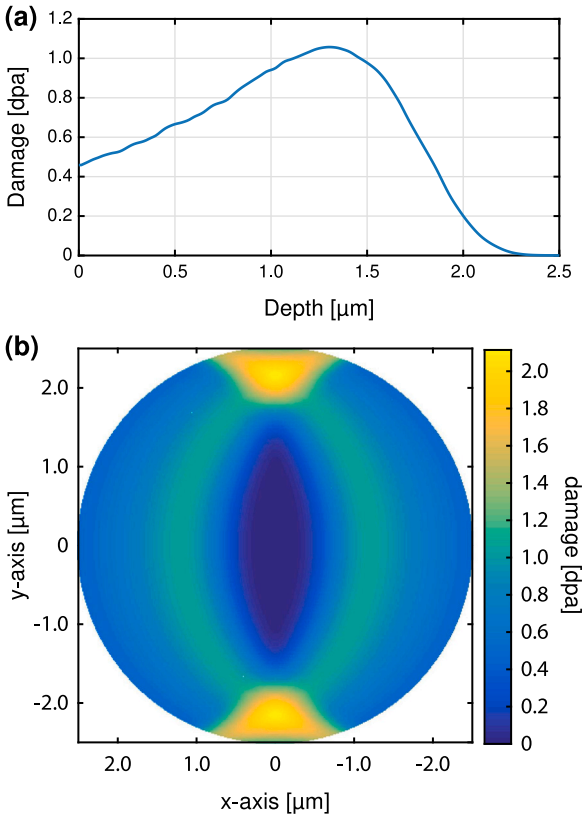

Fig. 3. (a) Damage depth profile caused by 20.5 MeV W ions in W at a fluence of 3.6×10^{14} cm^{-2} calculated with the 'Quick Calculation of Damage' option in SRIM [24] with a displacement energy threshold of 90 eV. The peak damage is at depth of 1.3 µm, the maximum penetration depth at approximately 2.3 µm (b) Damage profile in a W fibre with a diameter of 5 µm irradiated under these conditions from two opposite sides (for the visualisation 100 lines as shown in (a) were considered). In Table B.3 an overview of the area fraction per damage level is given.

probably remaining from the fabrication process and/or defects in the lacquer coating led to inhomogeneities in some cases. Only samples where the gauge length was free of those inhomogeneities were used for testing. The diameter was measured prior to testing by optical microscopy and for selected fibres after fracture at the undeformed part by scanning electron microscopy (SEM). In total nine samples met the requirements and were used for the investigation. Three were tested in the as-fabricated state and six samples were irradiated.

Samples were irradiated with a static W^{6+} beam in the TOF beam line of the 3 MV tandem accelerator at the Max-Planck-Institute for Plasmaphysics, Garching [37]. The beam profile can be approximated by a Gaussian with a width at half maximum of 2 mm. The samples were individually irradiated using an actively cooled copper sample holder. The thermal contact to the sample holder was ensured by a metal frame (opening 10 mm) or pins at both ends of the sample (distance 16 mm) that push the wire down. The sample holders are shown in Fig. A.7 in the appendix. The beam was targeted on the centre of the thinned part and was held static (no rastering). Due to the sufficient large beam size (see Table 1) the gauge section was irradiated completely. After a first irradiation, each sample was manually turned and irradiated again from the opposite side with the nominal same fluence. Fora 5 µm wire and a fluence of 3.6×10^{14} cm^{-2} this leads to the 2d damage profile shown in Fig. 3(b). This is defined as an average damage of 1 dpa as most of the wire, i.a. 74.5 %, receive a damage level between 0.5 and 1.5 dpa. The detailed values are given in Table B.3 in the appendix.

As a consequence of the energy input by the impinging ions, the samples are heated. For an approximation, we calculate the incoming heat based on ion energy, flux and projected area of the irradiated region for each sample. We assume heat conduction to the metal frame or pins (temperature 25 °C) and calculate the temperature using Fourier's law. We double-checked the results by a finite element calculation using Autodesk Simulation Mechanical 2017 for an ion flux of 3×10^{11} cm^{-2} s^{-1}. The energy deposited by the impinging ions was modelled as internal heat source where the ions are implanted into the material. Both heat transfer to the supports as well as heat radiation were considered.

The applied damage levels were 0.3 dpa, 1 dpa and 9 dpa, respectively (damage levels with respect to the definition of 1 dpa above). The damage levels were chosen to provide a large spread and correspond to estimated damage levels in a DEMO divertor (10 dpa for a Cu heat sink and 2 dpa for a W armor [38]). The actual ion flux was determined for each irradiation using a Faraday cup with a circular opening of 2 and 3 mm respectively. The irradiation time was then adjusted according to this flux and the desired damage level. For this study, the ion flux varied between 2 and 8×10^{11} cm^{-2} s^{-1}. The values for the individual samples are given in Table 1.

The tensile tests were performed with a universal testing machine (TIRA Test 2820) at room temperature. A 20 N load cell was used to measure the force in combination with a contact-less optical strain measurement system (details in [30]). In this system, the measuring length is defined by chosen reference points which were the transition points to the thinned centre region of the fibres. After mounting into the testing device, the paper frame was cut prior to tensile testing. The samples were preloaded to 5 mN and aligned using an x–y table. The tests were performed in a displacement controlled mode with a constant cross-head speed of 0.5 µm s^{-1}. The engineering stress was calculated using the measured load and the initial diameter of individual sample as given in Table 1. Engineering stress–engineering strain curves were derived using the measured strain and the calculated stress.

The fracture surface of all samples was investigated using a FEI Helios NanoLab 600 scanning electron microscope (SEM). As a measure of ductility, the reduction of area was determined for selected fibres using the SEM images.

Table 1
Overview of characteristics and test results for the individual irradiated samples. The uncertainty for strength and reduction in area results from the uncertainties in diameter measurements. The ion flux is given for both sides for an individual sample. Calibration measurements of the W flux give an absolute accuracy of better than 10 % [37]. As the damage is directly related to the ion flux we assume a similar error for the damage.

Actual diameter (measured) [μm]	*Ion flux (side1/side2)* [10^{11} cm^{-2} s^{-1}]	*Damage* [dpa]	*Beamspot (width x height)* [mm^2]	*Temperature (estimated)* [°C]	*Strength* [MPa]	*Reduction of area* [%]
8.5 ± 0.1	3.1/3.7	0.28	3 x 5	78	4015^{+96}_{-93}	52^{+6}_{-6}
6.6 ± 0.1	2.2/3.6	0.28	3 x 5	67	4310^{+134}_{-128}	56^{+6}_{-6}
5.7 ± 0.1	2.0/2.8	0.28	3 x 5	60	4986^{+180}_{-170}	51^{+6}_{-7}
5.4 ± 0.1	2.1/3.7	1.4	3 x 5	64	3248^{+124}_{-117}	60^{+5}_{-6}
5.4 ± 0.3	8.0/8.0	1.2	2 x 2	58	3998^{+432}_{-372}	58^{+8}_{-10}
3.8 ± 0.2	7.7/8.3	9.2	2 x 2	48	3480^{+376}_{-324}	60^{+7}_{-9}

Table 2
Summary of tensile test results calculated as the weighted mean. For comparison the value for 16 μm wire is given (taken from [30]).

Nominal diameter [μm]	*Damage* [dpa]	*Strength* [MPa]	*Reduction in area* [%]
16	–	4481 ± 35	49 ± 1
5	–	4080 ± 71	55 ± 3
5	0.3	4256 ± 70	53 ± 4
5	1	3310 ± 115	60 ± 5
5	9	3484[a]	60[a]

[a]Only one valid test.

4. Results

In Table 1, the detailed characteristics and test results for the irradiated samples are given. The ion flux is given for each side of the individual sample. The irradiation time was adjusted according to the actual flux in order to reach the anticipated damage (a fluence of 3.6 × 10^{14} cm^{-2} corresponds to 1 dpa). The actual fibre diameters after thinning differ from the desired diameter of 5 μm and from each other (compare also Fig. 5(c) and (d)). Depending on the actual fluence, beamsize and the used sample holder the calculated temperature varies between 48 and 78 °C. Although two samples have much larger ion flux, the temperature is quite similar due to the smaller beamspot. In contrast to that, the more realistic FEM calculation leads to a maximum temperature of 59 °C for the intermediate flux of 3 × 10^{11} cm^{-2} s^{-1}.

In Fig. 4, the engineering stress–strain curves of non-irradiated and ion-irradiated samples are shown. In both cases the curves show a clear ductile behaviour with yielding after elastic loading. There is a large scatter in the elastic slope, fracture strain as well as in the strength for the individual irradiation conditions. The strength varies between 3000 and 5000 MPa corresponding to loads between 60 and 100 mN (see Table 1 for concrete values). With respect to the uncertainties no clear trend is detectable although the strength seems to decrease rather than increase with damage. A similar trend seems to be valid for the yield point. In Fig. 5, corresponding fracture surfaces are shown. All fibres show the typical knife-edge fracture and a pronounced necking known for W wire [39,40]. No difference is visible for non-irradiated and irradiated material.

In Table 2, the mean strength and mean reduction in area are summarized. For comparison, also the value for a non-irradiated 16 μm wire is given (taken from [30]). The mean strength increases for 0.3 dpa and decreases afterwards but at the same time shows a large error. The reduction in area shows a very small spread and lies between 50 and 60 %.

5. Discussion

5.1. Measuring technique

Sample preparation by electropolishing allows a reduction of the diameter to the necessary dimension. However, the precision with which the final diameter is achieved is limited at the moment. As long as the actual diameter is measured with high accuracy and close to the location of final fracture the influence is expected to be low for strength and reduction of area as both is defined by the thinnest region. However, already small diameter variations along the gauge length could be a reason for the variations seen in the stress–strain curves (see Fig. 4). For example, a variation of the mean diameter of only 5 % due to inhomogeneous thinning would explain the deviation of the Young's Modulus in Fig. 4. On the other hand, the accuracy of the diameter measurement has a strong influence on the accuracy of the strength values due to a quadratic dependence. Another aspect which has to be considered when comparing the stress–strain curves is described in [30]. Due to the elastically stored energy in the testing system accelerated failure might occur and thus the strength is underestimated. This could be e.g. the case for sample number 6 in Fig. 4(d). These issues together with the very small load (depending on the diameter between 40 and 260 mN) and strain values make exact quantitative measurements difficult. A optimized method for diameter measurement as well as a load cell and a strain measuring system specifically designed for the small scale samples would be very beneficial.

The large beam size ensures the full irradiation of the sample and minimizes the risk of misalignment. However, as the beam shows a gaussian distribution a variation in the damage level along the fibre axis might still be present. A beam scanning along the fibre axis should be used to avoid this problem in the future. Calculations show that the sample only reaches moderate temperatures below 100 °C (compare Table 1). Even assuming a bad thermal contact, e.g. by isolating epoxy resulting from sample preparation, the temperature would in the worst case only reach 120 °C as calculated by the FEM model. This temperature region is far from any temperature where significant annihilation of irradiation defects or otherwise annealing of W is expected. Vacancies become mobile only above 280 °C [41] and only at temperatures well above 1400 °C full recovery sets in [42,43]. The presented procedure only allows sequential investigations. Simultaneous irradiation and loading could lead to different results due to synergistic effects, like they were reported for H retention [17,44]. Having an in-situ testing capability would in addition lower the risk of damaging the fragile samples during transfer. Therefore, a setup that allows irradiation and in-situ testing of such small samples is presently in development.

5.2. Conservation of ductility

All samples showed a ductile behaviour irrespective of the damage level. This can clearly be seen in the fracture surface (see Fig. 5) as well as in the yielding visible in the stress strain curves (see Fig. 4). In Fig. 6, an overview of the strength and reduction in area is given. There is a moderate decrease in strength with increasing damage level and thus no sign of irradiation hardening. The reduction in area stays more or less constant and even shows a slight increase. There is no reduction of ductility detectable.

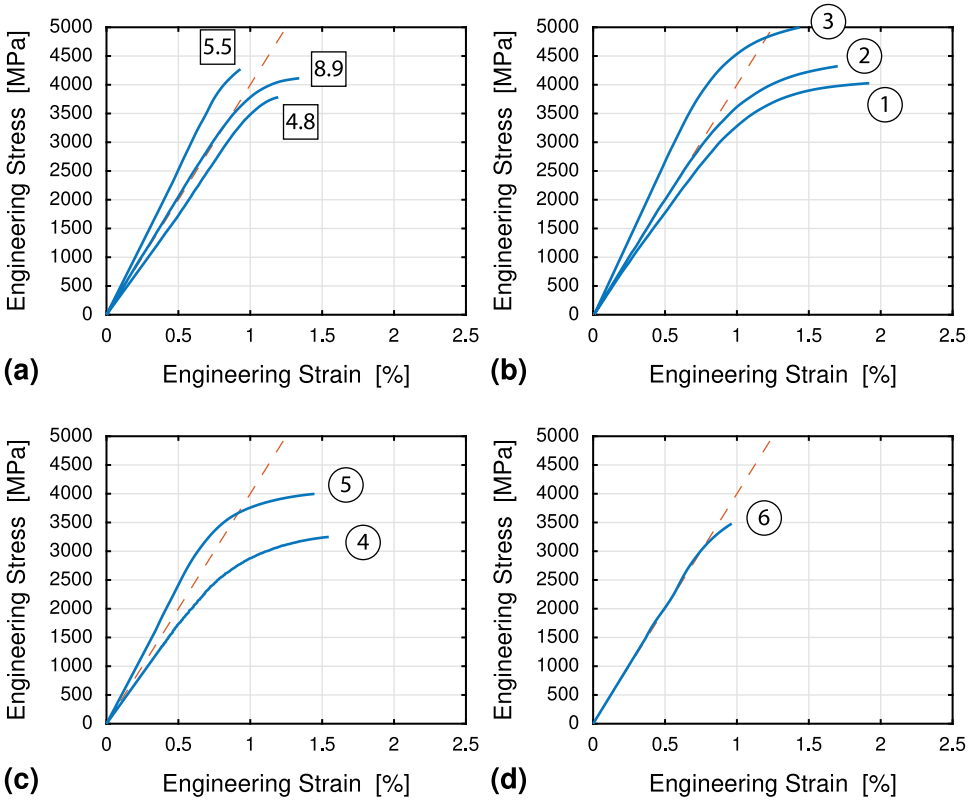

Fig. 4. Engineering stress–strain curves of tensile tests on drawn tungsten wire with a nominal diameter of 5 μm in (a) initial state and after irradiation to (b) 0.3 dpa, (c) 1 dpa and (d) 9 dpa. In (a) the diameter of the respective sample is given in the rectangular box. In (b–c) the numbers in the circles correspond to the respective sample in Table 1 (number corresponds to row). The curves were adjusted such that the elastic line starts in the origin and smoothed by a quadratic regression (MATLAB function: "smoothdata - rloess"). After elastic loading all samples show yielding and distinct plastic behaviour. The red dashed lines indicate an elastic deformation corresponding to a Young's modulus of 400 GPa.

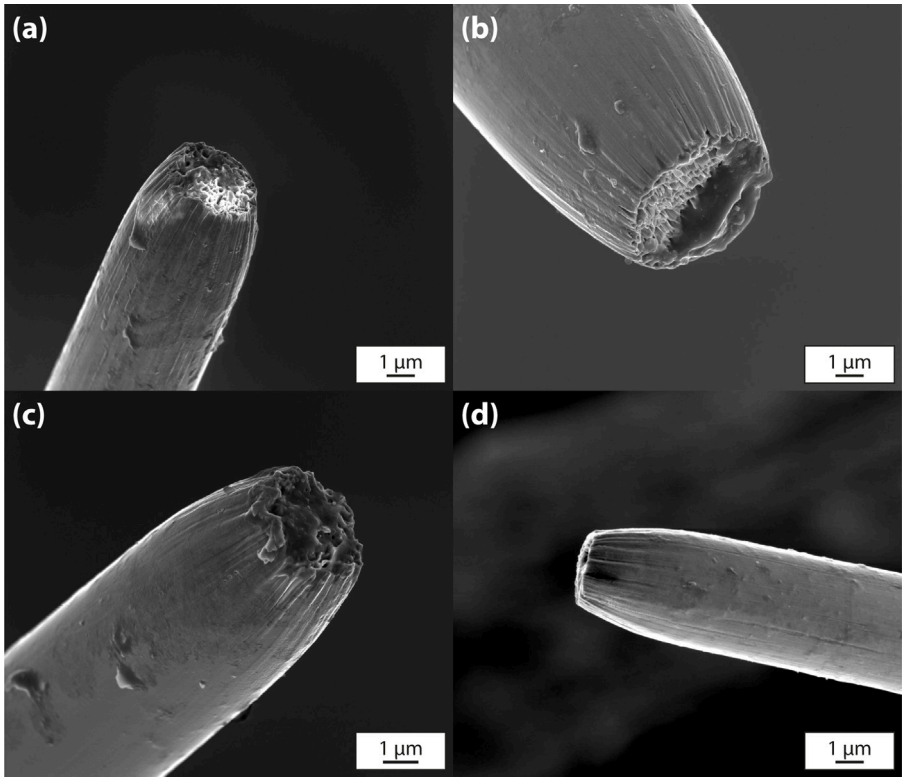

Fig. 5. Typical fracture surfaces of tensile tests on drawn tungsten wire with a diameter of 5 μm in (a) non-irradiated state and after irradiation to (b) 0.3 dpa, (c) 1 dpa and (d) 9 dpa. All samples show pronounced necking.

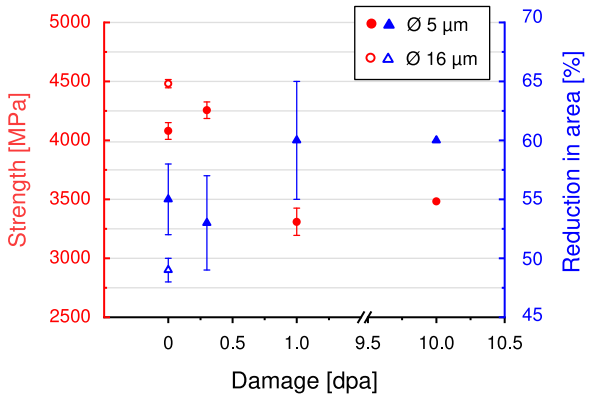

Fig. 6. Overview of strength (red circles) and reduction in area (blue triangles) for tungsten wire with a diameter of 16 µm (open symbols) and 5 µm (closed symbols) in the as fabricated case and for a diameter of 5 µm after irradiation.

A general problem for micromechanical testing is that at very low dimensions (i.e. below 10 µm) the uncertainties caused by the measurement system become proportionally more important. Here uncertainties in the diameter measurement have a large influence on the stress values (quadratic dependence) and thus complicate quantitative statements about hardening. However, hardening typically observed for tungsten increases to 34 % for ion-irradiated tungsten [27] and up to 100 % for neutron-irradiated samples [45] which should also be clearly visible in strength values. Regarding ductility, it has to be considered that the brittle to ductile transition (BDT) of the tungsten wire is well below RT (BDT of wire with a diameter of 250 µm occurs around −100 °C) [46]. Therefore, it might be that BDT did increase due to the radiation but has not yet reached room temperature and is hence not yet detectable. Measurements of the BDT of as-fabricated and irradiated samples are planned. However, BDT shifts of 600 °C have been observed for tungsten irradiated to 1 dpa in a fission reactor [47]. We can clearly exclude such a drastic increase in the present study.

The irradiation of the sample is not uniform (compare Table B.3) and most of the samples are thicker than the desired 5 µm. However, due to the circular shape the non-irradiated area is low up to a diameter of approximately 6 µm (approximately 80 % exhibit 25 % of the total dose or more). For the sample with a diameter of 8.5 µm the non-irradiated centre is more than 35 %, but no clear trend is obvious when comparing with thinner samples irradiated to the same dpa level (see Fig. 4(b)). The sample with highest damage rate does show a lower strength compared to the non-irradiated case although it is also the thinnest sample and thus exhibits full-depth irradiation. Therefore, we assume that the diameter variation does not conceal irradiation hardening. Since the use of thinner samples would be technically difficult to achieve, the use of lighter ions could lead to a more uniform irradiation of the entire volume. To avoid implantation of these ions the damage peak should be beyond the sample. In this case 3 MeV H ions would have a penetration depth of 20 µm and 6 MeV He ions would have a penetration depth of 8 µm (calculated by SRIM [24]). However, the use of lighter ions will lead to a reduction in dose rate (10^6 for H and 10^4 for He).

Nevertheless, a direct evidence of the irradiation damage in the microstructure would be helpful to get an idea about the uniformity. However, due to the already strongly distorted microstructure in the as-fabricated condition (see Fig. 1) the detection of damage is challenging. Transmission electron microscopy (TEM) is planned for as-fabricated and irradiated material. In addition, gentle heat treatment before irradiation can help to reduce the defect density in the as fabricated case (see e.g. [33,34]) and allow for easier detection of irradiation-caused damage.

Typically bulk tungsten shows distinct hardening [27,45] and loss of ductility [48] during irradiation. In neutron-irradiation experiments transmutation is suspected to play an important role for the change of mechanical behaviour. Therefore, the missing transmutation in this experiment could have reduced the effect of irradiation on the deformation behaviour. However, hardening was also observed for ion-irradiation. Another important effect might be that irradiation effects are not so pronounced in highly deformed and very fine grained material [49]. In the case of tungsten sheet material, Armstrong et al. [50] attributed this to the recombination of irradiation-caused point defects on subgrains which are caused by the high dislocation density. This is probably also true for the thin W wire as also the wire has a very fine microstructure (see Fig. 1). Walter et al. [51] showed that for drawn tungsten wire with a diameter of 63 µm the grain size is around 0.2 µm whereas for rod or sheet material showing irradiation hardening the average grain size is in the range of 10 µm and more [52].

Furthermore, thin W wire ($\varnothing \lesssim 1$ mm), although featuring a high dislocation density, exhibits distinct ductility as e.g. shown in [33] for as-fabricated wire. Whether this means that the deformation mechanism active in W wire is also less affected by defects induced by irradiation needs further investigation.

5.3. Consequences for the use in tungsten fibre-reinforced composites

In the case of W_f/W, the properties of the composite are dominated by the properties of the used wire [53]. Understanding the effect of irradiation on the tungsten wire can help describe the composite behaviour. At the moment, mainly wire with a diameter of 150 µm is used in W_f/W. The use of thinner wires down to a diameter of 16 µm is envisaged [54]. In [30], it was shown that the deformation behaviour of 150 µm wire is very similar to the thin wire. This means that even now the presented approach will help predicting the irradiation behaviour and help interpreting the results of irradiation studies [55] of W_f/W. The studies will be even more relevant once the thin wire is used in the composites.

Furthermore, the state of the wire influences the activation of extrinsic toughening mechanisms. A ductile fibre consumes crack energy by ductile deformation and is therefore more effective than a brittle fibre, which is rather being pulled out [56]. Because of this, the observed conservation of the ductility would be very beneficial for the composite toughness. In addition, due to the missing embrittlement the strength of the wire is preserved which is especially favourable for W_f/Cu.

6. Concluding remarks and outlook

Very thin W wire was irradiated by high-energy ions to DEMO-relevant damage levels. Due to the small size most of the volume is irradiated and the effect on mechanical properties could be studied using tensile testing. No significant change of the mechanical behaviour due to irradiation in terms of strength and ductility was observed. Using this technique, a systematic study of irradiation effects on the mechanical properties of thin W wire is now possible. This opens up possibilities for the further development of tungsten based composites and eventually helps to understand better the microscopic effects of irradiation.

It is planned to increase the number of tests and the dose to increase the statistical relevance of the results. To allow synergistic studies a tensile testing rig allowing mechanical tests in combination with ion beam loading is currently being developed. Here, the focus also lies in an optimized experimental setup e.g. a low load sensitive load cell and an improved and direct strain measurement.

Table B.3
Percentage of irradiated volume per dpa level as a result of the irradiation by 20.5 MeV W ions at a fluence of 3.6×10^{14} cm^{-2} from two sides (see profile given in Fig. 3). The first column gives the values for the target diameter of 5 µm, the other columns for the actual diameters of the tested samples. Sample numbers in last row correspond to samples in Table 1 and Fig. 4.

Damage δ in [dpa]	5.0 µm	3.8 µm	5.4 µm	5.7 µm	6.6 µm	8.5 µm
	Percentage in [%]					
$0.00 \le \delta < 0.01$	3.2	0	7.5	10.4	19.8	35.3
$0.01 \le \delta < 0.25$	8.3	0	9.0	9.7	9.2	8.3
$0.25 \le \delta < 0.50$	9.0	5.6	9.1	8.3	8.2	7.0
$0.50 \le \delta < 1.00$	57.0	56.3	54.2	53.1	47.5	38.3
$1.00 \le \delta < 1.50$	17.5	24.8	16.3	15.1	13.2	10.2
$1.50 \le \delta < 2.00$	4.4	11.6	3.4	2.9	1.8	0.8
$2.00 \le \delta$	0.6	1.7	0.5	0.4	0.3	0.1
Sample		6	4/5	3	2	1

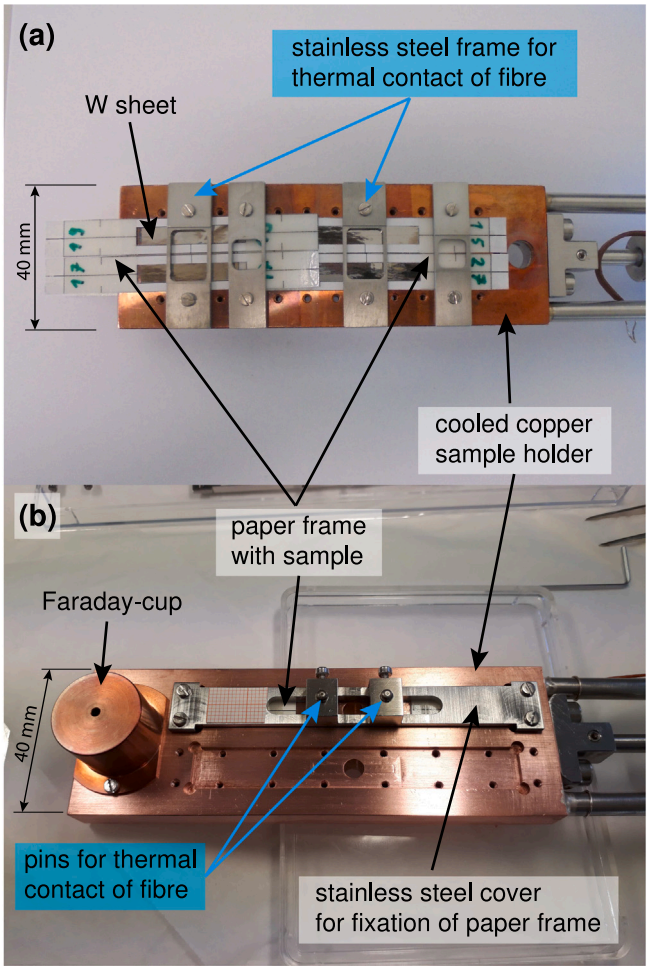

Fig. A.7. Sample holders used for irradiation. The holder shown in (a) was used for sample 1–4, the holder shown in (b) for sample 5 and 6 as given in Table 1. Both holders consist of a water cooled copper base and stainless steel covers to fix the samples. The thermal contact of fibre and base is ensured in (a) by the stainless steel cover and in (b) by pins pushing down the fibre. In (a) a tungsten sheet below the fibre prevents sputtering of the copper base.

CRediT authorship contribution statement

J. Riesch: Conceptualization, Methodology, Investigation, Formal analysis, Validation, Visualization, Writing – original draft, Supervision. **A. Feichtmayer:** Conceptualization, Methodology, Investigation, Formal analysis, Validation, Visualization, Writing – review & editing. **J.W. Coenen:** Writing – review & editing. **B. Curzadd:** Methodology, Writing – review & editing. **H. Gietl:** Methodology, Microscopy, Writing – review & editing. **T. Höschen:** Methodology, Investigation, Formal analysis, Writing – review & editing. **A. Manhard:** Methodology, Microscopy, Writing – review & editing. **T. Schwarz-Selinger:** Methodology, Investigation, Writing – review & editing. **R. Neu:** Writing – review & editing, Project administration, Funding acquisition.

Declaration of competing interest

The authors declare that they have no known competing financial interests or personal relationships that could have appeared to influence the work reported in this paper.

Acknowledgements

This work has been carried out within the framework of the EUROfusion Consortium and has received funding from the Euratom research and training programme 2014–2018 and 2019–2020 under grant agreement No 633053. The views and opinions expressed herein do not necessarily reflect those of the European Commission.

Appendix A. Sample holder

See Fig. A.7.

Appendix B. Damage fraction

See Table B.3.

References

[1] G. Federici, C. Bachmann, L. Barucca, C. Baylard, W. Biel, L.V. Boccaccini, C. Bustreo, S. Ciattaglia, F. Cismondi, V. Corato, C. Day, E. Diegele, T. Franke, E. Gaio, C. Gliss, T. Haertl, A. Ibarra, J. Holden, G. Keech, R. Kembleton, A. Loving, F. Maviglia, J. Morris, B. Meszaros, I. Moscato, G. Pintsuk, M. Siccinio, N. Taylor, M.Q. Tran, C. Vorpahl, H. Walden, J.H. You, Overview of the DEMO staged design approach in Europe, Nucl. Fusion 59 (6) (2019) 066013.
[2] J.W. Coenen, S. Antusch, M. Aumann, W. Biel, J. Du, J. Engels, S. Heuer, A. Houben, T. Hoeschen, B. Jasper, F. Koch, J. Linke, A. Litnovsky, Y. Mao, R. Neu, G. Pintsuk, J. Riesch, M. Rasinski, J. Reiser, M. Rieth, A. Terra, B. Unterberg, T. Weber, T. Wegener, J.-H. You, C. Linsmeier, Materials for DEMO and reactor applications—boundary conditions and new concepts, Phys. Scr. T167 (2016) 014002.
[3] G. Federici, W. Biel, M.R. Gilbert, R. Kemp, N. Taylor, R. Wenninger, European DEMO design strategy and consequences for materials, Nucl. Fusion 57 (9) (2017) 092002.
[4] S.W. Yih, C.T. Wang, Tungsten: Sources, Metallurgy, Properties, and Applications, Plenum Press, New York, 1979.
[5] J. Steichen, Tensile properties of neutron irradiated TZM and tungsten, J. Nucl. Mater. 60 (1) (1976) 13–19.

[6] S.A. Maloy, M.R. James, W. Sommer, G.J. Willcutt, M. Lopez, T.J. Romero, M.B. Toloczko, The effect of 800MeV proton irradiation on the mechanical properties of tungsten at room temperature and at 475°c, J. Nucl. Mater. 343 (1–3) (2005) 219–226.

[7] S.J. Zinkle, Applicability of copper alloys for DEMO high heat flux components, Phys. Scr. T167 (2016) 014004.

[8] C. Linsmeier, M. Rieth, J. Aktaa, T. Chikada, A. Hoffmann, J. Hoffmann, A. Houben, H. Kurishita, X. Jin, M. Li, A. Litnovsky, S. Matsuo, A. von Mueller, V. Nikolic, T. Palacios, R. Pippan, D. Qu, J. Reiser, J. Riesch, T. Shikama, R. Stieglitz, T. Weber, S. Wurster, J.-H. You, Z. Zhou, Development of advanced high heat flux and plasma-facing materials, Nucl. Fusion 57 (9) (2017).

[9] J. Riesch, Y. Han, J. Almanstötter, J.W. Coenen, T. Höschen, B. Jasper, P. Zhao, C. Linsmeier, R. Neu, Development of tungsten fibre-reinforced tungsten composites towards their use in DEMO—potassium doped tungsten wire, Phys. Scr. T167 (2016) 014006.

[10] Y. Mao, J.W. Coenen, J. Riesch, S. Sistla, J. Almanstötter, J. Reiser, A. Terra, C. Chen, Y. Wu, L. Raumann, T. Höschen, H. Gietl, R. Neu, C. Linsmeier, C. Broeckmann, Fracture behavior of random distributed short tungsten fiber-reinforced tungsten composites, Nucl. Fusion 59 (8) (2019) 086034.

[11] H. Gietl, S. Olbrich, J. Riesch, G. Holzner, T. Höschen, J.W. Coenen, R. Neu, Estimation of the fracture toughness of tungsten fibre-reinforced tungsten composites, Eng. Fract. Mech. 232 (2020) 107011.

[12] K.K. Chawla, Ceramic Matrix Composites, Springer US, Boston, MA, ISBN: 978-1-4757-2216-1, 1993.

[13] A. Müller, D. Ewert, A. Galatanu, M. Milwich, R. Neu, J.Y. Pastor, U. Siefken, E. Tejado, J.H. You, Melt infiltrated tungsten–copper composites as advanced heat sink materials for plasma facing components of future nuclear fusion devices, Fusion Eng. Des. 124 (2017) 455–459.

[14] A.V. Müller, B. Böswirth, V. Cerri, H. Greuner, R. Neu, U. Siefken, E. Visca, J.H. You, Application of tungsten–copper composite heat sink materials to plasma-facing component mock-ups, Phys. Scr. T171 (T171) (2020) 014015.

[15] S.J. Zinkle, J.T. Busby, Structural materials for fission & fusion energy, Mater. Today 12 (11) (2009) 12–19.

[16] G.S. Was, Fundamentals of Radiation Materials Science: Metals and Alloys, 2nd ed. 2017, Springer New York, New York, NY and s.l., ISBN: 9781493934362, 2017.

[17] S. Markelj, T. Schwarz-Selinger, M. Pečovnik, A. Založnik, M. Kelemen, I. Čadež, J. Bauer, P. Pelicon, W. Chromiński, L. Ciupinski, Displacement damage stabilization by hydrogen presence under simultaneous W ion damage and D ion exposure, Nucl. Fusion 59 (8) (2019) 086050.

[18] M.R. Gilbert, J.-C. Sublet, Neutron-induced transmutation effects in W and W-alloys in a fusion environment, Nucl. Fusion 51 (4) (2011) 043005.

[19] A. Hasegawa, M. Fukuda, K. Yabuuchi, S. Nogami, Neutron irradiation effects on the microstructural development of tungsten and tungsten alloys, J. Nucl. Mater. 471 (2016) 175–183.

[20] S. Das, Recent advances in characterising irradiation damage in tungsten for fusion power, SN Appl. Sci. 1 (12) (2019).

[21] O.V. Ogorodnikova, V. Gann, Simulation of Neutron-Induced Damage in Tungsten By Irradiation with Energetic Self-Ions, 2015, vol. 460.

[22] G.S. Was, R.S. Averback, Radiation damage using ion beams, in: R. Konings (Ed.), Comprehensive Nuclear Materials, Elsevier Science, Burlington, ISBN: 9780080560335, 2011, pp. 195–221, http://dx.doi.org/10.1016/B978-0-08-056033-5.00007-0.

[23] T. Mahmood, M. Griffiths, C. Lemaignan, R. Adamson, Material Test Reactors and other Irradiation Facilities, Advanced Nuclear Technology International, URL https://www.antinternational.com/docs/samples/FM/11/ZIRAT23_STR_Material_Test_Reactors_and_other_Irradiation_Facilities_Sample.pdf.

[24] J. Ziegler, J. Biersack, SRIM: The stopping range of ions in matter, URL http://www.srim.org.

[25] B. Wielunska, M. Mayer, T. Schwarz-Selinger, A. Sand, W. Jacob, Deuterium retention in tungsten irradiated by different ions, Nucl. Fusion 60 (9) (2020) 096002.

[26] E10 Committee, Practice for Neutron Radiation Damage Simulation by Charged-Particle Irradiation, ASTM International, West Conshohocken, PA, http://dx.doi.org/10.1520/E0521-16.

[27] D. Armstrong, C.D. Hardie, J. Gibson, A.J. Bushby, P.D. Edmondson, S.G. Roberts, Small-scale characterisation of irradiated nuclear materials: Part II nanoindentation and micro-cantilever testing of ion irradiated nuclear materials, J. Nucl. Mater. 462 (2015) 374–381.

[28] A. Prasitthipayong, Small-scale mechanical testing and size effects in extreme environments, engineering - materials science and engineering, (Ph.D. thesis), University of California, Berkeley, 2017, URL https://escholarship.org/uc/item/6sc4c0z8#main.

[29] P. Hosemann, C. Shin, D. Kiener, Small scale mechanical testing of irradiated materials, J. Mater. Res. 30 (9) (2015) 1231–1245.

[30] J. Riesch, A. Feichtmayer, M. Fuhr, J. Almanstötter, J.W. Coenen, H. Gietl, T. Höschen, C. Linsmeier, R. Neu, Tensile behaviour of drawn tungsten wire used in tungsten fibre-reinforced tungsten composites, Phys. Scr. T170 (2017) 014032.

[31] J. Riesch, J. Almanstötter, J.W. Coenen, M. Fuhr, H. Gietl, Y. Han, T. Höschen, C. Linsmeier, N. Travitzky, P. Zhao, R. Neu, Properties of drawn w wire used as high performance fibre in tungsten fibre-reinforced tungsten composite, IOP Conf. Ser.: Mater. Sci. Eng. 139 (2016) 012043.

[32] P. Schade, 100Years of doped tungsten wire, Int. J. Refract. Met. Hard Mater. 28 (6) (2010) 648–660.

[33] P. Zhao, J. Riesch, T. Höschen, J. Almanstötter, M. Balden, J.W. Coenen, R. Himml, W. Pantleon, U. von Toussaint, R. Neu, Microstructure, mechanical behaviour and fracture of pure tungsten wire after different heat treatments, Int. J. Refract. Met. Hard Mater. 68 (2017) 29–40.

[34] V. Nikolić, J. Riesch, M.J. Pfeifenberger, R. Pippan, The effect of heat treatments on pure and potassium doped drawn tungsten wires: Part II – Fracture properties, Mater. Sci. Eng. A 737 (2018) 434–447.

[35] W.F. Hosford, Microstructural changes during deformation of [011] fiber-textured metals, Trans. Metall. Soc. AIME (230) (1964) 12–15.

[36] A. Manhard, U. von Toussaint, M. Balden, S. Elgeti, T. Schwarz-Selinger, L. Gao, S. Kapser, T. Płociński, J. Grzonka, M. Gloc, Ł. Ciupiński, Microstructure and defect analysis in the vicinity of blisters in polycrystalline tungsten, Nucl. Mater. Energy 12 (2017) 714–719.

[37] T. Schwarz-Selinger, Deuterium Retention in MeV Self-Implanted Tungsten: Influence of Damaging Dose Rate, 2017, vol. 12.

[38] J.H. You, G. Mazzone, E. Visca, C. Bachmann, E. Autissier, T. Barrett, Cocilovo, F. Crescenzi, P.K. Domalapally, Dongiovanni, S. Entler, G. Federici, P. Frosi, M. Fursdon, H. Greuner, Hancock, Marzullo, S. McIntosh, A.V. Müller, M.T. Porfiri, G. Ramogida, J. Reiser, M. Richou, M. Rieth, A. Rydzy, R. Villari, Widak, Conceptual design studies for the European DEMO divertor: Rationale and first results, Fusion Eng. Des. 109–111 (2016) 1598–1603.

[39] S. Leber, J. Tavernelli, D.D. White, R.F. Hehemann, Fracture modes in tungsten wire, J. Less Common Met. 48 (1) (1976) 119–133.

[40] D. Terentyev, L. Tanure, A. Bakaeva, A. Dubinko, V. Nikolić, J. Riesch, K. Verbeken, S. Lebediev, E.E. Zhurkin, Micromechanical and microstructural properties of tungsten fibers in the as-produced and annealed state: Assessment of the potassium doping effect, Int. J. Refract. Met. Hard Mater. 81 (2019) 253–271.

[41] J. Heikinheimo, K. Mizohata, J. Räisänen, T. Ahlgren, P. Jalkanen, A. Lahtinen, N. Catarino, E. Alves, F. Tuomisto, Direct observation of mono-vacancy and self-interstitial recovery in tungsten, APL Mater. 7 (2) (2019) 021103.

[42] M. Zibrov, T. Dürbeck, W. Egger, M. Mayer, High temperature recovery of radiation defects in tungsten and its effect on deuterium retention, Nucl. Mater. Energy 23 (2020) 100747.

[43] F. Ferroni, X. Yi, K. Arakawa, S.P. Fitzgerald, P.D. Edmondson, S.G. Roberts, High temperature annealing of ion irradiated tungsten, Acta Mater. 90 (2015) 380–393.

[44] T. Schwarz-Selinger, J. Bauer, S. Elgeti, S. Markelj, Influence of the Presence of Deuterium on Displacement Damage in Tungsten, 2018, vol. 17.

[45] T. Miyazawa, L.M. Garrison, J.W. Geringer, M. Fukuda, Y. Katoh, T. Hinoki, A. Hasegawa, Neutron irradiation effects on the mechanical properties of powder metallurgical processed tungsten alloys, J. Nucl. Mater. 529 (2020) 151910.

[46] L.L. Seigle, C.D. Dickinson, Effect of mechanical and structural variables on ductile-brittle transition in refractory metals, Refractory Metals and Alloys II, Refract. Met. Alloy. II 17 (1963) 65–116.

[47] E. Gaganidze, A. Chauhan, H.-C. Schneider, D. Terentyev, G. Borghmans, J. Aktaa, Fracture-mechanical properties of neutron irradiated ITER specification tungsten, J. Nucl. Mater. 547 (2021) 152761.

[48] L.M. Garrison, Y. Katoh, N.K. Kumar, Mechanical properties of single-crystal tungsten irradiated in a mixed spectrum fission reactor, J. Nucl. Mater. 518 (2019) 208–225.

[49] I.J. Beyerlein, A. Caro, M.J. Demkowicz, N.A. Mara, A. Misra, B.P. Uberuaga, Radiation damage tolerant nanomaterials, Mater. Today 16 (11) (2013) 443–449.

[50] D.E. Armstrong, T.B. Britton, Effect of dislocation density on improved radiation hardening resistance of nano-structured tungsten–rhenium, Mater. Sci. Eng. A 611 (2014) 388–393.

[51] J.L. Walter, E.F. Koch, The relationship of microstructure to mechanical properties of Al-, Si-, K-doped tungsten wire, J. Mater. Sci. 26 (2) (1991) 505–509.

[52] D. Terentyev, C. Yin, A. Dubinko, C.C. Chang, J.H. You, Neutron irradiation hardening across ITER diverter tungsten armor, Int. J. Refract. Met. Hard Mater. 95 (2021) 105437.

[53] H. Gietl, J. Riesch, J.W. Coenen, T. Höschen, C. Linsmeier, R. Neu, Tensile deformation behavior of tungsten fibre-reinforced tungsten composite specimens in as-fabricated state, Fusion Eng. Des. 124 (2017) 396–400.

[54] H. Gietl, A.V. Müller, J.W. Coenen, M. Decius, D. Ewert, T. Höschen, P. Huber, M. Milwich, J. Riesch, R. Neu, Textile preforms for tungsten fibre-reinforced composites, J. Compos. Mater. 52 (28) (2018) 3875–3884.

[55] G. Pintsuk, E. Diegele, S.L. Dudarev, M. Gorley, J. Henry, J. Reiser, M. Rieth, European materials development: Results and perspective, Fusion Eng. Des. 146 (2019) 1300–1307.

[56] J. Riesch, J.-Y. Buffiere, T. Höschen, M. Scheel, C. Linsmeier, J.-H. You, Crack bridging in as-fabricated and embrittled tungsten single fibre-reinforced tungsten composites shown by a novel in-situ high energy synchrotron tomography bending test, Nucl. Mater. Energy 15 (2018) 1–12.